



# GLYCINE-RICH RNA-BINDING PROTEIN 7 potentiates effector-triggered immunity through an RNA recognition motif

Octavina C. A. Sukarta <sup>1</sup>, Qi Zheng <sup>1</sup>, Erik J. Sloopweg <sup>1</sup>, Mark Mekken<sup>1</sup>, Melanie Mendel <sup>1</sup>, Vera Putker<sup>1</sup>, André Bertran <sup>1</sup>, Anouk Brand <sup>1</sup>, Hein Overmars <sup>1</sup>, Rikus Pomp<sup>1</sup>, Jan Roosien<sup>1</sup>, Sijf Boeren <sup>2</sup>, Geert Smart <sup>1</sup> and Aska Goverse <sup>1,\*†</sup>

- 1 Laboratory of Nematology, Wageningen University & Research, Wageningen, The Netherlands
- 2 Laboratory of Biochemistry, Wageningen University & Research, Wageningen, The Netherlands

\*Author for correspondence: [aska.goverse@wur.nl](mailto:aska.goverse@wur.nl)

These authors contributed equally (O.C.A.S. and Q.Z.)

†Senior author

A.G. is responsible for conceptualization of this work; O.C.A.S. and Q.Z. for methodology; O.C.A.S., Q.Z., E.J.S., J.R., S. B., H.O., R.P., Ma.M., Me.M., V.P., A. Be., and A.Br. were involved in investigation. O.C.A.S. wrote the original draft; Q.Z. wrote the revised draft; O.C.A.S., Q.Z., A.G., and G.S. were involved in writing, review, and editing; A.G. helped in funding acquisition.

The author responsible for distribution of materials integral to the findings presented in this article in accordance with the policy described in the Instructions for Authors (<https://academic.oup.com/plphys/pages/general-instructions>) is Aska Goverse ([aska.goverse@wur.nl](mailto:aska.goverse@wur.nl)).

## Abstract

The activity of intracellular plant nucleotide-binding leucine-rich repeat (NB-LRR) immune receptors is fine-tuned by interactions between the receptors and their partners. Identifying NB-LRR interacting proteins is therefore crucial to advance our understanding of how these receptors function. A co-immunoprecipitation/mass spectrometry screening was performed in *Nicotiana benthamiana* to identify host proteins associated with the resistance protein Gpa2, a CC-NB-LRR immune receptor conferring resistance against the potato cyst nematode *Globodera pallida*. A combination of biochemical, cellular, and functional assays was used to assess the role of a candidate interactor in defense. A *N. benthamiana* homolog of the GLYCINE-RICH RNA-BINDING PROTEIN7 (NbGRP7) protein was prioritized as a Gpa2-interacting protein for further investigations. NbGRP7 also associates in planta with the homologous Rx1 receptor, which confers immunity to Potato Virus X. We show that NbGRP7 positively regulates extreme resistance by Rx1 and cell death by Gpa2. Mutating the NbGRP7 RNA recognition motif (RRM) compromises its role in Rx1-mediated defense. Strikingly, ectopic NbGRP7 expression is likely to impact the steady-state levels of Rx1, which relies on an intact RRM. Our findings illustrate that NbGRP7 is a pro-immune component in effector-triggered immunity by regulating Gpa2/Rx1 function at a posttranscriptional level.

## Introduction

The plant innate immune system is orchestrated by a consortium of cell-autonomous receptor proteins (Bezerra-Neto et al., 2020). On the cell surface, pattern recognition

receptors detect conserved pathogen-associated molecular patterns (PAMPs) or damage inflicted on the host (danger-associated molecular pattern; Jones and Dangl, 2006; Zipfel, 2014). This triggers basal defense coined as PAMP-triggered

immunity (PTI). Pathogens, however, can adapt by evolving virulence-promoting effector molecules to disarm PTI and/or interfere with other host cellular processes (Jones and Dangl, 2006). In this interplay, plants evolved resistance proteins (R proteins), the majority of which belongs to the family of nucleotide-binding leucine-rich repeat (NB-LRR) receptors (Bezerra-Neto et al., 2020). Classical NB-LRRs modules have a tri-domain architecture consisting of a central Nucleotide-Binding APAF-1, R-Protein, and CED4 (NB-ARC) region flanked by an N-terminal domain (typically a coiled-coil [CC] or toll/interleukin receptor-like (TIR) domain) and a C-terminal LRR domain (van der Biezen and Jones, 1998a, 1998b; Jones et al., 2016). NB-LRRs act as a molecular switch that can readily toggle between ADP-bound inactive and ATP-bound active states (Takken et al., 2006). The switch function is triggered by recognition of race-specific effector molecules to trigger effector-triggered immunity (ETI). ETI can effectively limit pathogen ingress and is often hallmarked by the visible sign of programmed cell death (Balint-Kurti, 2019). However, the sequence of events leading to immunity remains largely unresolved.

Plant NB-LRRs engage in various interactions with other components in the host proteome, either as preformed complexes or as an active response to a pathogenic intrusion (Sun et al., 2020). The common view is that these interactions modulate immunity by regulating defense signaling and/or affecting the stability, localization, or activity of the receptor (Sacco et al., 2009; Sukarta et al., 2016; Sun et al., 2020; van Wersch et al., 2020). In a vast majority of cases, binding to these co-factors is mediated by domains at the receptor's N-terminal end (Sun et al., 2020). This is also consistent with reports showing that the CC/TIR domains of a few NB-LRR systems can multimerize upon activation, which is thought to increase the surface area available for scaffolding interacting partners (Bentham et al., 2018). The nature of proteins known to bind to an NB-LRR varies, ranging from well-established molecular-chaperones (e.g. SGT1 and RAR1) to transcription factors (Bieri et al., 2004; de la Fuente van Bentem et al., 2005; Leister et al., 2005; Taming and Baulcombe, 2007; Chang et al., 2013; Townsend et al., 2018). Aside from a few exceptions, however, a limited number of host proteins are known to directly associate with the NB-LRR N-termini (Sun et al., 2020). Additionally, how these interactors contribute to NB-LRR immunity is often not fully understood. Uncovering the identity and functions of these interactors will contribute to advancing our understanding of how NB-LRRs mediate defense.

The CC domain of the potato R protein Rx1, which confers resistance to Potato Virus X (PVX), has been shown to act as a scaffold by recruiting various molecular components (Sacco et al., 2007; Taming and Baulcombe, 2007; Townsend et al., 2018; Sukarta et al., 2020). In the cytoplasm, Rx1 forms a complex with RanGTPase-activating protein 2 (RanGAP2) to retain a subpopulation of the receptor in this compartment. This is required by Rx1 to recognize PVX and prompt a complete defense response to the virus (Slootweg

et al., 2010; Taming et al., 2010). A pool of Rx1 also resides in the nucleus, where it co-opts and modulates the DNA-binding activity of nuclear-associated proteins such as the Golden2-like transcription factor (GLK1) and DNA-Binding Bromodomain Containing Protein (DBCP; Townsend et al., 2018; Sukarta et al., 2020). The recruitment of compartment-specific host proteins is thought to grant Rx1 with distinct cellular functions as a molecular sensor and response factor. The CC domain of Gpa2, which mediates defense against the potato cyst nematode *Globodera pallida*, shares considerable homology with the Rx1-CC (95.7% similarity at the protein level). Despite bearing substantial similarities, however, the Gpa2-CC has only been reported to associate with RanGAP2 (Taming and Baulcombe, 2007). Whether Gpa2 shares a more extensive pool of interacting components in the nucleus and/or cytoplasm is unknown. Elucidating this will reveal the degree by which homologous NB-LRR receptors diverge in their signaling components. This will in turn, uncover common, critical points for regulating NB-LRR activity.

In this study, we identified a *Nicotiana benthamiana* homolog of the GLYCINE-RICH RNA-BINDING PROTEIN 7 (NbGRP7) as an interactor of Gpa2. GRP7s are highly conserved plant proteins involved in RNA processing and have previously been implicated in early and late PTI responses (Lee et al., 2012; Nicaise et al., 2013; Wang et al., 2020). However, the function of a GRP7 homolog in ETI has yet to be reported. Here, we present molecular evidence that NbGRP7 is a pro-immunity component in effector-induced immune responses by Gpa2 and Rx1. Substituting a conserved arginine residue in the NbGRP7 RNA recognition motif (RRM) compromises its potentiating effects on Rx1-mediated resistance, suggesting that RNA-binding may be crucial for the function of NbGRP7 in NB-LRR-mediated immunity. Additionally, we show that NbGRP7 regulates the steady-state levels of Rx1 transcripts and, as a consequence, proteins in the cell. Our results collectively reveal a layer of control on the activity of intracellular NB-LRR immune receptors, like Gpa2 and Rx1, at a posttranscriptional level.

## Results

### Identification and isolation of NbGRP7 as a Gpa2-interacting protein

To screen for putative interactors of the Gpa2-CC domain, we adopted a targeted proteomics approach by performing cellular fractionation coupled with co-immunoprecipitation/mass spectrometry (Co-IP/MS) analysis in *N. benthamiana*. To that end, Gpa2-CC-GFP or GFP (negative control) bait constructs were generated under the control of the Cauliflower Mosaic Virus promoter for transient overexpression in *N. benthamiana* by *Agrobacterium tumefaciens* transient assay (ATTA). As anticipated, Mass Spectrometry analysis of the eluted fractions showed an overrepresentation of the Gpa2-CC-GFP bait in both cellular extracts. We also co-purified RanGAP2 exclusively in the cytoplasmic fraction of the pull-down consistent with previous studies

(Sacco et al., 2007; Tameling and Baulcombe, 2007). This finding supports that the technical approach and stringency used for the data analysis were sound. From the list of candidate interactors, a protein was selected that has substantial peptide hits matching to a GRP7 homolog which co-precipitated consistently with the Gpa2-CC nuclear fraction (Supplemental Fig S1; Supplemental Table S1). Given the specificity and reproducibility of the interaction observed, we prioritized GRP7 in further studies as described below.

To facilitate functional analysis, we isolated the predicted *N. benthamiana* GRP7 (NbGRP7) homolog based on the *N. benthamiana* draft genome (Solgenomics) and existing AtGRP7 sequence. The isolated transcript is 501-bp long, encoding a protein of 167 amino acids with an estimated weight of ~16.9 kDa. Additional sequence alignment showed that NbGRP7 exhibits strong similarity with other plant-derived GRPs, sharing the highest sequence identity (73%–75% at the amino acid level) to the *Solanum tuberosum* GRP7 variants (XP\_006365106.1 and XP\_006365107.1) (Supplemental Figure S2A). The NbGRP7 N-terminus constitutes the most conserved region, wherein the canonical RRM resides (Supplemental Figure S2B). Positioned within this region are also two Ribonucleoprotein motifs (RNP1 and RNP2) and arginine residues required for RNA binding (summarized schematically in Figure 1A; Fu et al., 2007; Nicaise et al., 2013). The variable and highly disordered glycine-rich region accounts for the remaining C-terminal half of the protein, which is further interspersed with aromatic amino acids.

### NbGRP7 interacts with full-length Gpa2 and Rx1 in planta via the CC domain

We next sought to confirm the interaction identified in the Co-IP/MS screening by performing bimolecular fluorescence complementation (BiFC) imaging. Although NbGRP7 was originally found to associate with the Gpa2-CC domain, we expanded our assay to test the interaction of NbGRP7 with Rx1 given its close homology (88% similarity at amino acid level), particularly in the CC which only differs in six amino acid residues. To that end, we created both Gpa2-CC and Rx1-CC constructs fused to the N-terminal half of the super cyan fluorescent protein SFCFP3A (pN:G1 and pN:R1) for transient co-expression with NbGFP7, which was fused to the C-terminal half of SFCFP3A (pC:NbGRP7). The reverse combinations (pC:R1, pC:G1, and pN:NbGRP7) were also generated for comparison. Combinations co-expressing pN:R1 or pN:G1 with the viral protein NSs (pC:NSs) were used as negative controls. Likewise, the combination of NbGRP7 with  $\beta$ -Glucuronidase (pN:GUS) was used as an additional negative control. Confocal imaging at 2 days postinfiltration (dpi) shows that a CFP signal accumulated in the nucleus and to a lesser extent, in the cytoplasm when either pN:G1 or pN:R1 was co-expressed with pC:NbGRP7 (Figure 1B). Remarkably, detailed imaging of the nuclei showed the nucleoplasm to have a nonhomogeneous distribution with CFP signals accumulating in subnuclear bodies

similar to those described in earlier studies of AtGRP7 (Kim et al., 2008). These cellular structures are typically associated with RNA processing which coincides with the expected function of a GRP7 homolog (Spector and Lamond, 2011). Conversely, a CFP signal was absent upon co-expression of the negative control combinations (pN:R1/pN:G1 with pC:NSs and pC:NbGRP7 with pN:GUS; Figure 1B). All aforementioned constructs were expressed stably and similar results were obtained with the reverse combinations (Supplemental Figure S3, A and B). Combined, our findings confirm that NbGRP7 can form a complex with the CC domains of Gpa2 and Rx1 in planta, predominantly in the nucleus.

We next examined whether NbGRP7 can bind to full-length Gpa2 and Rx1 in planta by Co-IP. Thus, a 4 $\times$ Myc.GFP-NbGRP7 construct was co-expressed transiently in combination with (HA)-tagged version of the full-length receptors (4 $\times$ HA-Gpa2 and Rx1-4 $\times$ HA.GFP). Infiltrated leaf materials were harvested at 2 dpi and the extracted proteins were subjected to a Co-IP using the  $\alpha$ -HA magnetic beads system ( $\mu$ MACS). Immunoblotting of the eluates shows that 4 $\times$ Myc.GFP-NbGRP7 co-precipitates with both 4 $\times$ HA-Gpa2 and Rx1-4 $\times$ HA.GFP (Figure 1C). A smaller size band was detected below 4 $\times$ Myc.GFP-NbGRP7, which was often noticed under our protein extraction conditions and this might be caused by degradation of 4 $\times$ Myc.GFP-NbGRP7. Consistent with the Co-IP/MS screening, we also observed 4 $\times$ Myc.GFP-NbGRP7 to specifically co-purify with the CC-domain of Gpa2 (4 $\times$ HA-Gpa2-CC). Taken together, our data demonstrate that NbGRP7 protein interacts with full-length Gpa2 and Rx1 immune receptors in planta.

To further localize the structural determinants in the CC required for NbGRP7 binding, we used available S1 and S4 surface mutants of the Rx1-CC domain as described in Sloomweg et al. (2018). The S4 mutations disrupt the hydrophobic patch essential for RanGAP2-binding in helix 4 of the Rx1-CC, while the S1 mutations in helix 1 reduce intramolecular binding to the NB-LRR. We showed that 4 $\times$ Myc.GFP-NbGRP7 co-precipitated with the S1 and S4 mutant variants (CC and full-length) similar to the wild-type (WT) control (Supplemental Figure 4, A and B). While the immunoblot shows that Rx1 S1-4 $\times$ HA.GFP pulled down at a greater extent compared to the WT and S4 derivatives (Supplemental Figure 4B), this was not consistent between experimental repeats. These findings suggest that S1 and S4 surface regions of the CC are most likely not involved in complex formation with NbGRP7. Thus, NbGRP7 interacts with Rx1-CC at a surface region distinct from those required for intramolecular interactions and RanGAP2 binding.

### NbGRP7 is a positive regulator of effector-dependent defenses by Gpa2 and Rx1

To ascertain the biological relevance of the interaction observed for NbGRP7 and Rx1/Gpa2, we performed a cell death assay in *N. benthamiana* leaves. Agrobacteria harboring 4 $\times$ Myc.GFP-NbGRP7 were co-infiltrated with Rx1/Gpa2

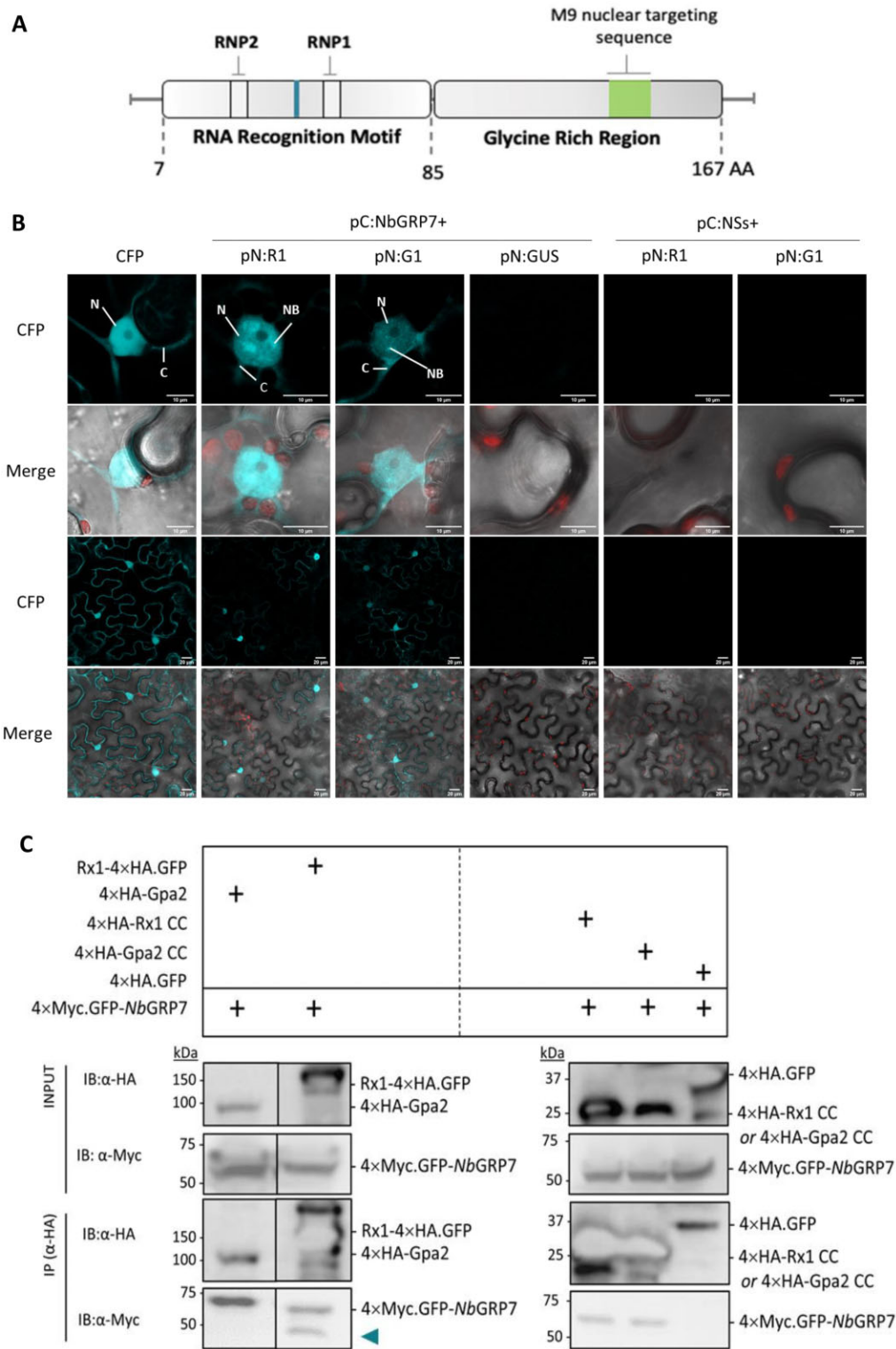


**Figure 1** Identification of NbGRP7 as Gpa2 and Rx1-interacting protein. A, Schematic diagram representing the full-length NbGRP7 homolog isolated from *N. benthamiana* cDNA. The conserved Arginine residue required for RNA binding is highlighted. B, BiFC of SCFP3A. The N-terminal half of the super cyan fluorescent protein SCFP3A fused to Rx1-CC or Gpa2-CC (pN:R1 or pN:G1) and the C-terminal half of SCFP3A fused to NbGRP7 (pC:NbGRP7) were co-expressed in *N. benthamiana* leaves. SCFP3A was detected in CFP channel, chlorophyll auto-fluorescence was shown together with CFP signal in the merged channel. Free CFP was used as positive control and co-expression with pC:NSs or pN:GUS were used as negative controls. N, nucleus. C, cytoplasm. NB, nuclear body. Scale bar = 10 or 20 μm. Cells were imaged at 2 dpi based on three cells. Results are representative of two biological repeats. C, Immunoblots from Co-IP of NbGRP7 with full-length Gpa2/Rx1 or their CC domains. For the pull-downs, crude extracts of *N. benthamiana* co-expressing the appropriate protein combinations were incubated with α-HA magnetic beads (μMACS). Gpa2/Rx1 constructs or the negative 4×HA.GFP control were used as baits to co-purify 4×Myc.GFP-NbGRP7. Considering different size of HA-tagged protein, the HA blot was separated into two parts (Rx1/Gpa2 full length in left and the CC domain in right) for better detection and result display. 4×Myc.GFP of the NbGRP7 fusion construct sometimes tends to be cleaved-off under the protein extraction conditions used. This is indicated by the triangle.

and their matching effectors, namely the coat protein of PVX strain UK3 (PVX-CP UK3) and GpRBP-1 variant D383-1, respectively. Infiltrated spots were monitored for the progression of cell death within 3–5 dpi by measuring chlorophyll loss. Interestingly, transiently overexpressing 4×Myc.GFP-NbGRP7 potentiates GpRBP-1-induced cell death by Gpa2 (under the control of its endogenous promoter) at 5 dpi as indicated by a greater chlorophyll loss compared to the GFP control (Figure 2A). To determine whether the pro-immunity functions of NbGRP7 were effector-dependent, we also included an autoactive p35S:Gpa2 D460V construct. Interestingly, 4×Myc.GFP-NbGRP7 overexpression does not influence autoactivity by p35S:Gpa2 D460V. These results show that NbGRP7 specifically contributes to effector-induced cell death.

For Rx1, cell death is typically a quick response in *N. benthamiana*. We, therefore, compared cell death induced by Rx1 constructs cloned under the endogenous (pRx1), CaMV35S (p35S), or leaky scan promoter (p35<sub>LS</sub> as described in Slootweg et al. (2010)). Contrary to Gpa2, transient overexpression of 4×Myc.GFP-NbGRP7 had negligible effects on Rx1-mediated cell death at 3 dpi (Figure 2B). No significant differences in chlorophyll loss relative to the control could be observed reproducibly when overexpressing 4×Myc.GFP-NbGRP7, PVX-CP UK3, and Rx1, irrespective of the immune receptor construct used. Likewise, NbGRP7 overexpression did not influence the autoactivity of an pRx1:Rx1D460V construct. Contrary to Gpa2, NbGRP7 does not contribute to Rx1-mediated cell death responses in this study under the conditions used for testing.

Notably, cell death is viewed as a secondary latent response for Rx1 that is reserved by the host when immunity proves insufficient, for example, when there is an overabundance of the viral coat protein such as during heterologous expression assays (Bendahmane et al., 1999). Instead, PVX infection typically induces an extreme resistance response, which can effectively restrict viral spread without the need to elicit cell death (Bendahmane et al., 1995; Bhattacharjee et al., 2009). We, therefore, investigated the impact of NbGRP7 overexpression on extreme resistance by Rx1. *Nicotiana benthamiana* leaves were infiltrated with Agrobacteria harboring an amplicon of the avirulent PVX-UK3 strain and p35<sub>LS</sub>:Rx1. Viral levels were quantified by DAS-ELISA within 1–5 dpi. Our data demonstrate that NbGRP7 enhances Rx1-mediated extreme resistance against PVX-UK3 between 3 and 5 dpi, as shown by a significantly greater reduction in viral levels compared to the control (Figure 2C). Collectively, these findings indicate that NbGRP7 positively regulates extreme resistance by Rx1. We further show that overexpressing NbGRP7 reduces PVX-UK3 accumulation in the absence of p35<sub>LS</sub>:Rx1 (Supplemental Figure S5), consistent with existing studies implicating the role of AtGRP7 in basal defense (Lee et al., 2012). These results combined illustrate a role for NbGRP7 in both Rx1-dependent and -independent defenses against PVX.

To complement our overexpression studies, Tobacco Rattle Virus (TRV)-Virus Induced gene Silencing (VIGS) silencing of NbGRP7 was performed. However, TRV-VIGS-silenced plants showed severe developmental phenotypes at 3 weeks postsilencing (Supplemental Figure S6), most likely due to pleiotropic effects of NbGRP7 silencing on accumulation of TRV. We, therefore, abandoned this approach and alternatively, performed local transient hairpin silencing of NbGRP7 (Shin et al., 2017). Hairpin constructs (denoted as hpNbGRP7) were designed to knockdown transcript levels of endogenous NbGRP7 specifically upon leaf infiltration (Supplemental Figure S7). Similar p35<sub>LS</sub>:Rx1 and PVX-UK3 combinations as described above were co-infiltrated with hpNbGRP7, and virus levels were quantified at 3 dpi. The results demonstrate that transient silencing of NbGRP7 leads to significantly higher accumulation of PVX-UK3, indicating that Rx1-dependent resistance was hampered (Figure 2D). These findings complement our overexpression analysis and collectively, support the role of NbGRP7 in extreme resistance by Rx1. Taken together, our data demonstrate that NbGRP7 acts a pro-immune component in Gpa2 and Rx1-mediated effector-dependent defenses.

### The function of NbGRP7 in Rx1-mediated extreme resistance depends on an intact RRM

Having established a role of NbGRP7 in Gpa2 and Rx1 immunity, we questioned whether its capacity to bind RNA may underly the observed phenotypes. Thus, we mutated a conserved arginine residue at position 49 of the NbGRP7 RRM to generate mutant variants (NbGRP7-R49K or -R49Q) impaired in their RNA binding as described in (Nicaise et al., 2013). Immunoblotting indicates that 4×Myc.GFP-NbGRP7 R49K and 4×Myc.GFP-NbGRP7 R49Q are expressed as stably as WT 4×Myc.GFP-NbGRP7 (Supplemental Figure S8A). We also compared the subcellular distribution patterns to WT NbGRP7 using confocal microscopy. Interestingly, the mutant variants showed different cellular distribution patterns as the subnuclear bodies characteristic of NbGRP7 were considerably less prominent (Supplemental Figure S8B).

We then assessed the effects of overexpressing 4×Myc.GFP-NbGRP7 R49K and 4×Myc.GFP-NbGRP7 R49Q on the Rx1-mediated extreme resistance response as described above. Quantification of virus levels by Double Antibody Sandwich (DAS)-Enzyme-linked Immunosorbent Assay (ELISA) showed that both mutants still potentiate PVX-UK3-induced extreme resistance at 3 dpi, although significantly less than WT NbGRP7 (Figure 3A). To corroborate these findings, Real Time (RT)-qPCR analysis was performed, which indicates that levels of viral transcripts increased in tissues where p35<sub>LS</sub>:Rx1 was co-expressed with the mutants compared to WT NbGRP7 (Figure 3, B and C). These results combined suggest that the function of NbGRP7 in Rx1-dependent defenses rely on an intact RNA-binding domain.

To confirm whether the NbGRP7 mutant variants still interact with Rx1, a Co-IP was performed using similar experimental set-ups as described beforehand.

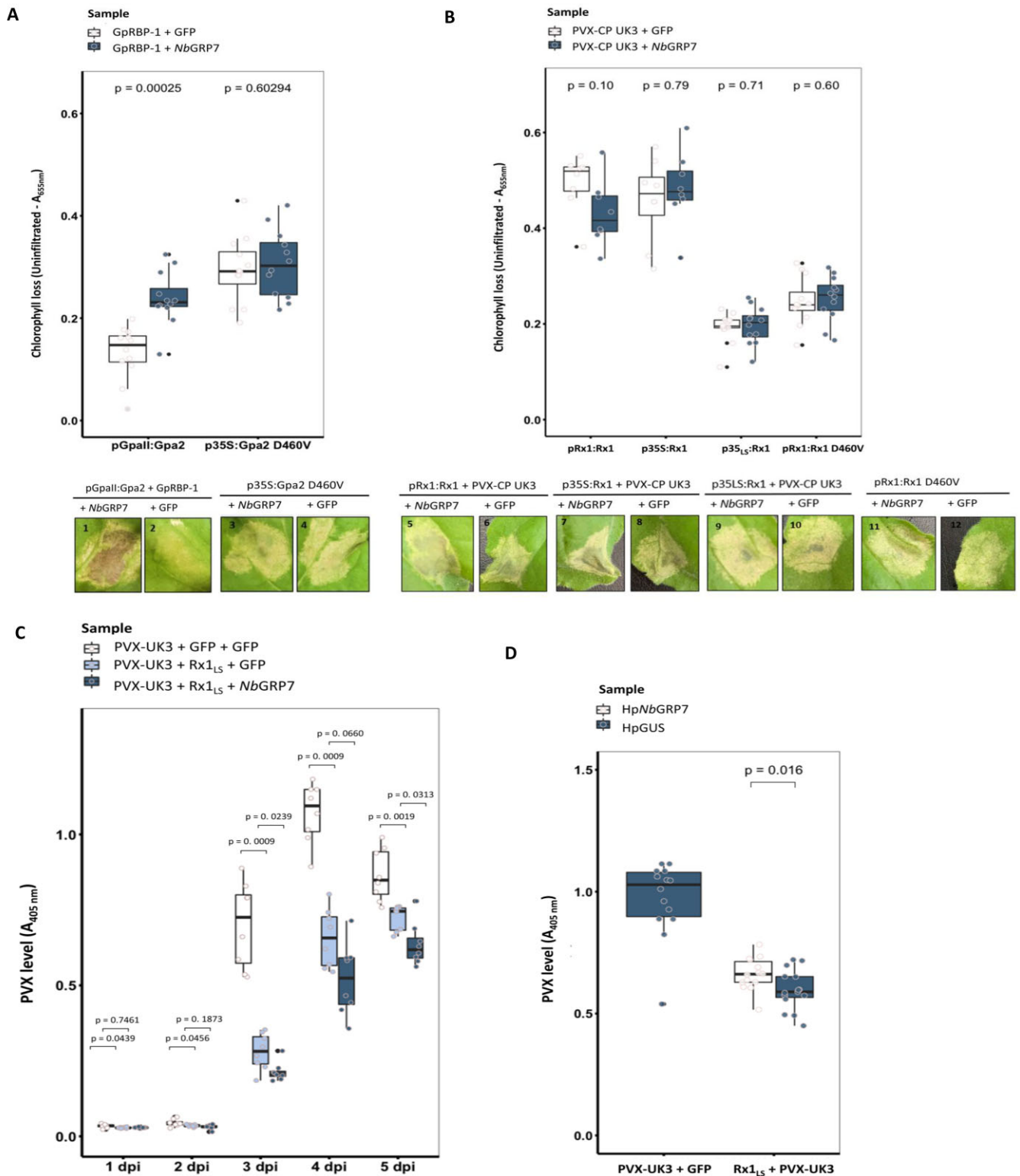


**Figure 2** NbGRP7 potentiates defenses by Gpa2 and Rx1. Boxplots representing Gpa2- (A) and Rx-1 (B) mediated chlorophyll loss of elicitor-induced or independent cell death upon overexpression of NbGRP7 at 3–5 dpi. Bars represent the interquartile range while the cross indicates the median. The whiskers mark the minimal and maximal data points. Significance was calculated using Wilcoxon-Signed Rank test with  $\alpha = 0.05$  from  $n \geq 12$  samples. Data shown are representative of at least three independent repeats. For the cell death assay, constructs of Rx1 under the control of either a 35S, endogenous, or leaky scan promoter was used, whereas Gpa2 was cloned under the control of its endogenous promoter (pGpal1). Representative photographs of infiltrated leaf zones are provided in the next row. Boxplots of absorbance at 405 nm, indicating levels of PVX avirulent strain (PVX-UK3) upon transient overexpression (C) or silencing (D) of NbGRP7 in the context of Rx1-mediated responses. Data shown are representative of at least three independent repeats with similar results. Significance was calculated using Wilcoxon-Signed Rank test with  $\alpha = 0.05$  from  $n \geq 8$  samples.

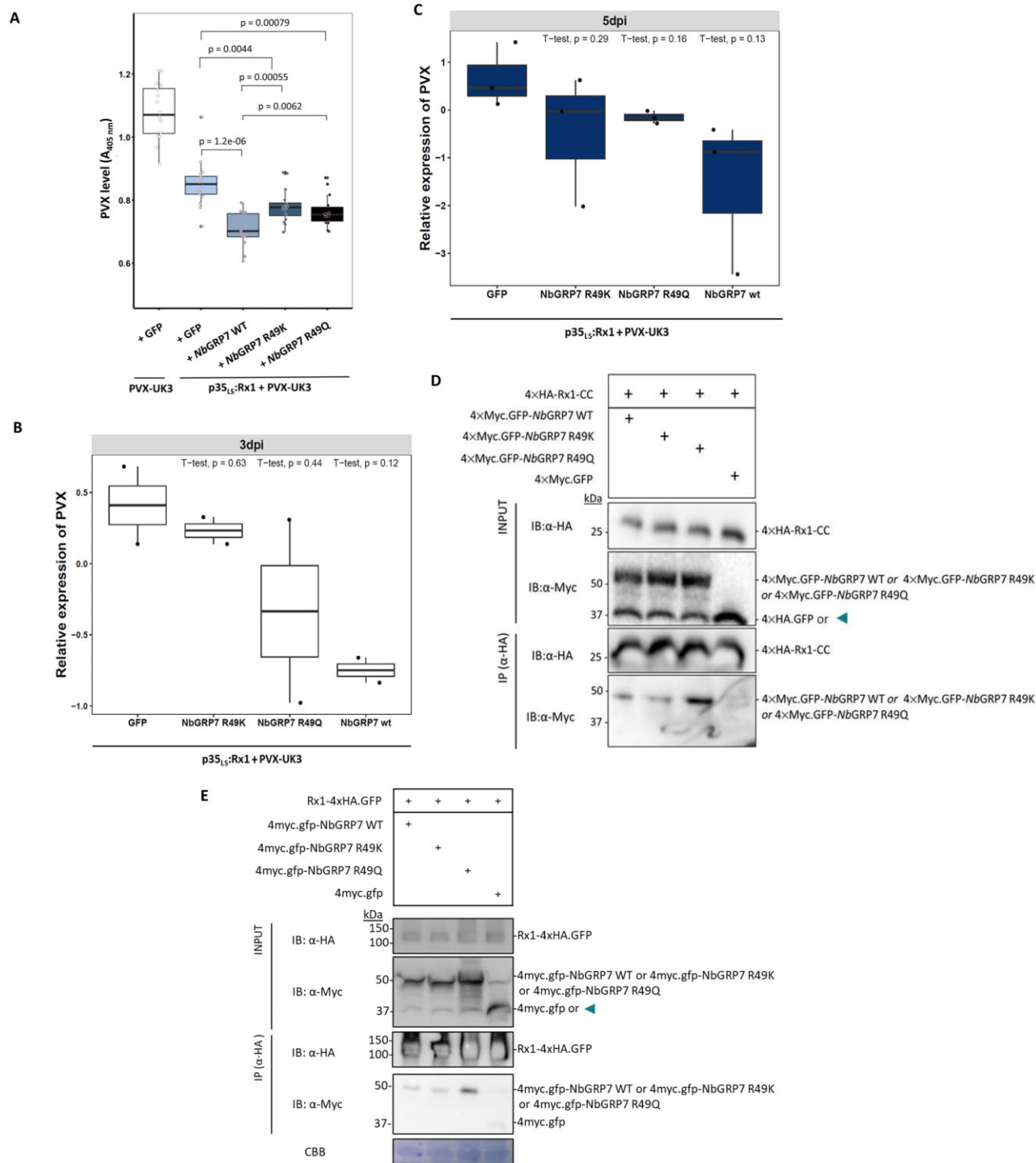


**Figure 3** The RNA-binding activity of NbGRP7 contributes to Rx1-mediated extreme resistance against PVX avirulent strain (PVX-UK3) in *N. benthamiana*. **A**, Boxplots of a double antibody sandwich ELISA (DAS-ELISA) assay from transient overexpression of p35<sub>L5</sub>:Rx1-GFP and PVX-UK3 in combination with 4xMyc.GFP-NbGRP7 WT, NbGRP7 R49K, or NbGRP7 R49Q. Bars represent the interquartile range, and the cross indicates the median. The whiskers mark the minimal and maximal data points. Statistical significance was calculated using Wilcoxon-Signed Rank test with  $\alpha = 0.05$  from  $n \geq 12$  samples. **B** and **C**, Boxplots of RT-qPCR analysis of viral transcript levels as determined using primers specific for the PVX coat protein. RNA from infected *N. benthamiana* leaves harvested at 3 dpi (**B**) and 5 dpi (**C**) were used for the analysis. Data shown are combination of two (**B**) or three (**C**) biological repeat experiments, with each sample consisting of a pool of at least five different plants. To obtain the relative fold change, samples were first normalized to the actin reference gene and then compared to the combination of Rx1<sub>L5</sub> + PVX-UK3 + GFP. Bars represent the interquartile range, and the cross indicates the median. The whiskers mark the minimal and maximal data points. Statistical significance was calculated using *t* test. **D** and **E**, Co-IP of HA-tagged Rx1-CC domain or the full-length immune receptor in combination with WT or mutated variants of 4xMyc.GFP-NbGRP7.  $\alpha$ -HA beads were used to pull-down the receptor fragments. The success of the Co-IP is detected in the  $\alpha$ -Myc immunoblot. “+” indicates the presence of a particular construct in the infiltration combination. Cleaved 4xMyc.GFP-NbGRP7 under the extraction conditions is indicated by the triangle.

Immunoblotting shows that 4×Myc.GFP-NbGRP7 R49K co-immunoprecipitated at comparable levels with 4×HA-Rx1-CC and 4×HA-Rx1 as the WT NbGRP7 (Figure 3, D and E). Thus, we concluded that the reduced pro-immune activity of NbGRP7 R49K is not due to a lack of complex formation with the Rx1-CC, but most likely from the loss of its RNA-binding capacity. Notably, however, the NbGRP7 R49Q variant pulled-down consistently to a greater extent than WT NbGRP7. Thus, substituting the conserved arginine residue in NbGRP7 to an amino acid with markedly different properties enhanced its physical interaction with Rx1. Coupled with our functional data, this suggests that the contribution of NbGRP7 in Rx1 defense may also rely on its interaction with the immune receptor.

### NbGRP7 seems to maintain the steady-state levels of Rx1 in planta

Our data show that NbGRP7 strengthens Rx1-mediated extreme resistance is dependent on an intact RRM. This suggests that the RNA chaperone activity of NbGRP7 may underlie its function in Rx1-mediated defense, for example, by the stabilization of Rx1 transcripts as described for AtGRP7 and FLS2 (Nicaise et al., 2013). To explore this model, we investigated whether overexpressing and silencing of NbGRP7 affects mRNA levels of Rx1 in the cell by performing RT-qPCR analysis. Our findings show that the relative abundance of Rx1 transcripts increased upon NbGRP7 overexpression in the absence of PVX by ca two- to four-fold when compared to the GFP control at 3 and 5 dpi (Figure 4A). Conversely, silencing NbGRP7 decreased Rx1 transcript levels. We reproduced these assays under activating conditions of Rx1 by PVX-UK3. Similar changes in Rx1 transcript profiles were observed during immune activation by PVX-UK3 (Figure 4B). These findings combined show that NbGRP7 can modulate the steady-state transcript levels of Rx1 in the cell.

If NbGRP7 stabilizes Rx1 transcripts, we anticipated that this would result in a concomitant increase in Rx1 protein levels. Indeed, immunoblotting assays shows that overexpression of 4×Myc.GFP-NbGRP7 led to higher protein accumulation of p35<sub>L5</sub>:GFP-Rx1 while NbGRP7 silencing reduced this amount (Figure 4, E and F). Moreover, we could demonstrate that this increase in Rx1 transcript and protein abundance depends on the RNA-binding capacity of GRP7. Upon overexpression of the NbGRP7 RNA-binding mutants NbGRP7 R49K and NbGRP7 R49Q, reduced transcript and protein levels of Rx1 were observed when compared to WT NbGRP7 both in the presence and absence of PVX-UK3 (Figure 4, C and D). Collectively, our findings indicate that NbGRP7 stabilizes the steady-state level of Rx1, which could explain its pro-immune activity in Rx1-mediated plant defense as described.

### Endogenous GRP7 is downregulated upon PVX or *G. pallida* infection

As NbGRP7 contributes to Rx1- and Gpa2-mediated immune response, we were curious how NbGRP7 itself is regulated upon pathogen infection. Therefore, we first examined GRP7 transcript levels upon PVX infection. We co-infiltrated p35<sub>L5</sub>:Rx1 and NbGRP7 with or without PVX-UK3 to check NbGRP7 regulation. NbGRP7 transcript level was quantified via RT-qPCR at both 3 and 5 dpi. Upon PVX-UK3 infection, NbGRP7 transcript levels were upregulated at 3 dpi and dropped at 5 dpi (Figure 5A). In addition, we tested endogenous NbGRP7 regulation upon PVX-UK3 infection at both 3 and 5 dpi. This also resulted in reduced levels of endogenous NbGRP7 upon PVX-UK3 infection but now already from 3 dpi onwards (Figure 5B). These data show that NbGRP7 is downregulated upon PVX infection.

Next, we also analyzed the impact of PCN infection on endogenous GRP7 transcript levels. For this, we used potato as a host for nematode infection since *G. pallida* cannot infect roots of *N. benthamiana*. We infected the Gpa2-resistant potato genotype SH with the *G. pallida* avirulent population D383 and virulent population Rookmaker. Infected root segments were harvested at 3 and 6 dpi for assessment of GRP7 transcript levels via RT-qPCR. To identify the NbGRP7 homolog in potato, we blasted the NbGRP7 sequence against the potato genome database (PGSC DM v4.03 genes) in Solgenomics and got only one matching candidate PGSC0003DMG400000708, which is annotated as Glycine-rich RNA-binding protein and referred to from here onwards as StGRP7 (Supplemental Figure 9). Data showed that upon *G. pallida* infection, StGRP7 showed downregulation at both 3 and 6 dpi (Figure 5C), indicating that also upon *G. pallida* infection GRP7 transcript levels are reduced consistent with NbGRP7 regulation during PVX infection. Moreover, StGRP7 displayed a comparable transcript level in D383 and Rookmaker-infected samples at both 3 and 6 dpi, suggesting StGRP7 gene expression is suppressed by *G. pallida* in both the compatible and incompatible interaction. Overall, our data demonstrate that endogenous GRP7 gene expression is downregulated upon infection of either PVX or *G. pallida* in two different plant species, *N. benthamiana* and potato respectively, probably to promote virulence by suppressing the GRP7 pro-immune response.

### Discussion

The activity of plant NB-LRRs is regulated by their interaction with components in the plant proteome. However, the identities and functions of NB-LRR-associated proteins are largely unknown. In this study, we describe the identification of NbGRP7 as an interactor of the intracellular NB-LRR immune receptors Gpa2 and Rx1 based on a Co-IP/MS screening in *N. benthamiana*. Transient overexpression and silencing experiments demonstrate that NbGRP7 positively contributes to GpRBP-1-dependent cell death by Gpa2 and extreme resistance by Rx1. Interestingly, ectopically

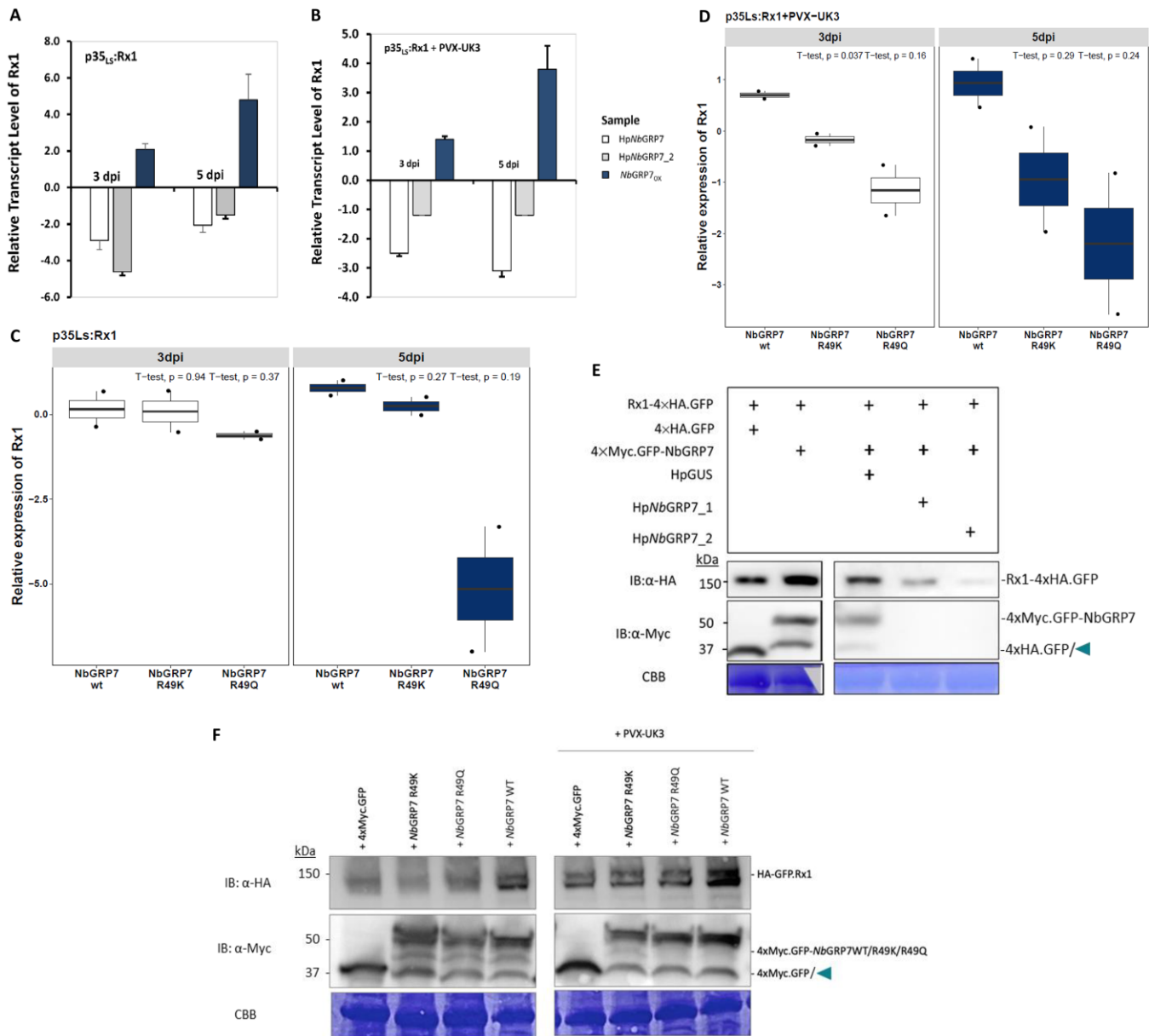


**Figure 4** NbGRP7 regulates Rx1 transcript abundance pre- and postactivation by PVX avirulent strain (PVX-UK3). A and B, RT-qPCR showing expression profile of Rx1 transcript co-expressed with a construct, whereby NbGRP7 is either overexpressed or silenced in *N. benthamiana* upon activation by PVX-UK3 or in the absence of the pathogen. Leaf samples were harvested at either 3 or 5 dpi. For each combination shown, data was obtained from a pool of at least five different plants. Rx1 transcript levels were normalized to the actin reference gene and the fold change was calculated relative to HpGUS (for hairpin silencing experiments) or GFP-GUS (for NbGRP7 overexpression experiments). Error bars represent the standard error. C and D, Boxplots of RT-qPCR quantifying the relative transcript abundance of Rx1 pre- and postactivation in the presence of WT or mutant NbGRP7 constructs at 3 or 5 dpi. Data shown are based on the combination of two biological repeat experiments. Fold change was derived following normalization to the actin reference gene and compared to the combination containing WT NbGRP7. Bars represent the inter-quartile range, and the cross indicates the median. The whiskers mark the minimal and maximal data points. Statistical significance was calculated using *t* test. E, Ectopic expression of NbGRP7 affects the protein abundance of Rx1. Immunoblot of protein extracts from *N. benthamiana* leaves co-expressing full-length Rx1 in combination with left) 4xMyc.GFP, 4xMyc.GFP-NbGRP7 or right) 4xMyc.GFP-NbGRP7 with the hairpin silencing constructs. Leaf samples were harvested at 3 dpi. Data shown are from a single representative experiment. CBB-stained membrane of the RUBisCO protein served as loading control. The missing corner of the left CBB-stained membrane was cut as a position mark. F, Immunoblot demonstrating the protein stability of full-length HA.GFP-Rx1 in combination with the overexpression of 4xMyc.GFP, 4xMyc.GFP-NbGRP7, 4xMyc.GFP-NbGRP7 R49Q, or 4xMyc.GFP-NbGRP7 R49K in the absence (left) or presence (right) of PVX-UK3. Data shown are from a single representative experiment. CBB-stained membrane of the RUBisCO protein served as loading control. Cleavage of 4xMyc.GFP of the NbGRP7 fusion construct under the extraction conditions is indicated by the triangle.

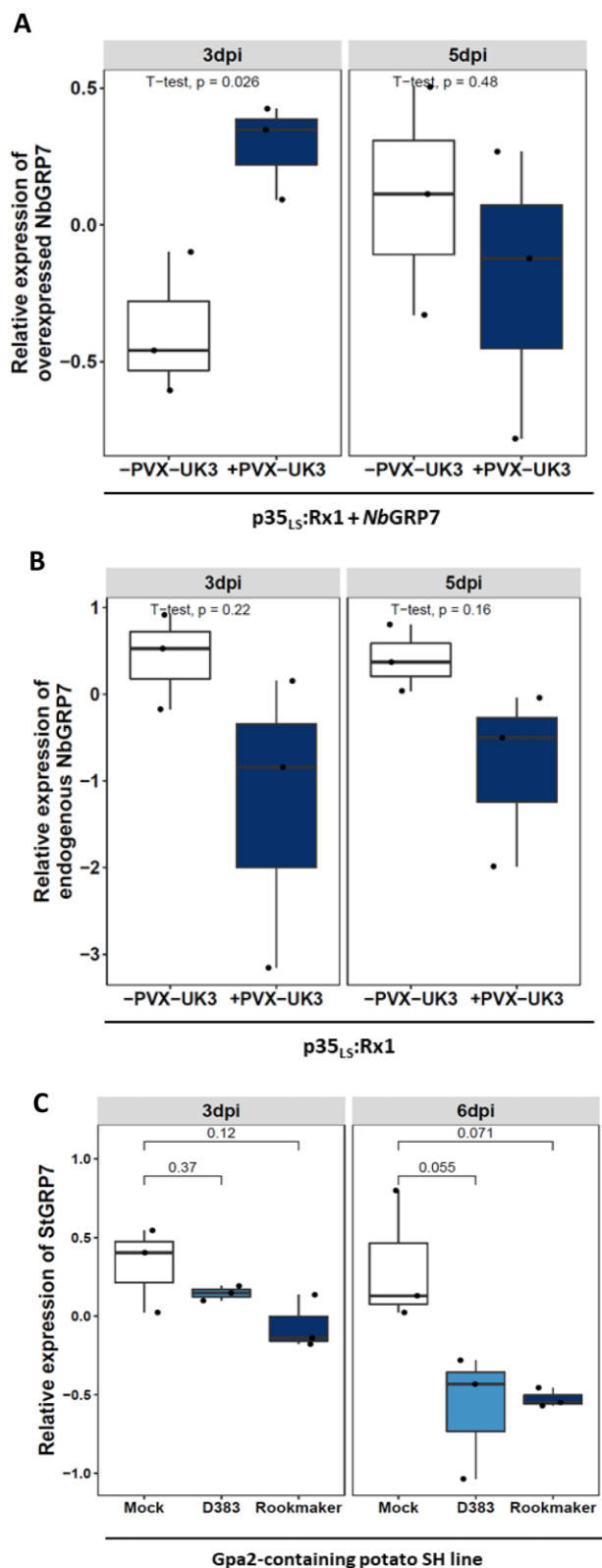


**Figure 5** NbGRP7 regulation upon PVX or *G. pallida* infection. A and B, Boxplots of RT-qPCR analysis of NbGRP7 transcript levels upon avirulent strain PVX-UK3 infection. Total RNA from infected *N. benthamiana* leaves harvested at 3 and 5 dpi were used for the analysis. A, Overexpressed NbGRP7 transcript. B, Endogenous NbGRP7 transcript. Data shown are the combination of three biological experiments. NbGRP7 transcript levels were normalized to the actin reference gene

expressing NbGRP7 also influenced Rx1 transcript and protein abundance. Both the pro-immune activity and transcript regulation of Rx1 by NbGRP7 rely on an intact RNA-binding domain. Taken together, we infer that NbGRP7 acts as a co-factor regulating the stability of its NB-LRR receptors. We postulate that this occurs at a posttranscriptional level, which is an underexplored mechanism for fine-tuning the functioning of plant NB-LRRs like Gpa2/Rx1. Our research elucidates the role of a GRP7 homolog in ETI.

In contrast, a role for GRP7 has been explored extensively in the context of basal immunity. For instance, the RNA-binding function of Arabidopsis (*Arabidopsis thaliana*) GRP7 (AtGRP7) is targeted by the *Pseudomonas syringae* effector HopU1 for ADP-ribosylation to promote virulence of the bacteria (Fu et al., 2007). A more recent study implicates that the phosphorylation of AtGRP7 induces a dynamic and global alternative splicing response in the Arabidopsis transcriptome upon activation of the FERONIA receptor (Wang et al., 2020). Combined with our data, this indicates that PTI and ETI recruit the same pro-immune components present in plant cells to activate defense. This supports the idea that PTI and ETI involve (partial) overlapping pathways in plant immunity. Interestingly, we demonstrate in this study that NbGRP7 can enhance basal resistance against PVX, consistent with the role of AtGRP7 in FLS2- and FERONIA-mediated defenses (Supplemental Figure S5; Lee et al., 2012; Nicaise et al., 2013; Wang et al., 2020). Our findings, therefore, illustrate that NbGRP7 is a shared component of PTI and ETI. A parallel can also be drawn with GLK1, which also interacts with the CC domain and potentiates both Rx1-extreme resistance and basal resistance against PVX (Townsend et al., 2018). In hindsight, this showed that a single NB-LRR protein can tap into hubs of defense signaling, which fit within a general picture of convergent cell surface-localized and intracellular immune signaling pathways in plant defense.

We demonstrated that NbGRP7 is a pro-immune component of both GpRBP-1-triggered cell death by Gpa2 and extreme resistance by Rx1 in *N. benthamiana* (Figure 2, A–D). NbGRP7 thus adds to the pool of shared co-factors of Rx1 and Gpa2 immunity aside from RanGAP2 (Sacco et al., 2007; Tameling and Baulcombe, 2007). These findings suggest that Rx1 and Gpa2 may converge in their use of co-factors and

#### Figure 5 (Continued)

and then compared to the combination without PVX-UK3 infection. C, Boxplots of StGRP7 transcript levels upon *G. pallida* infection. Potato resistance genotype SH line was infected with *G. pallida* virulent population (Rookmaker) and avirulent population (D383) and infected root segments were harvested at 3 and 6 dpi for RT-qPCR analysis. Inoculation without *G. pallida* was performed as Mock group. Data shown is consisted of three biological experiments. StGRP7 transcript levels were normalized to the RPN7 and TUA5 reference genes and then compared to the mock group. Bars represent the interquartile range, and the cross indicates the median. The whiskers mark the minimal and maximal data points. Statistical significance was calculated using *t* test.

signaling requirements despite their different recognition specificities. This is consistent with sequence exchange experiments showing that the CC-NB of Gpa2 can replace the CC-NB of Rx1 and vice versa while remaining immune receptor function (Slootweg et al 2017). It is striking to note that NbGRP7 overexpression did not affect the autoactive response of Gpa2/Rx1 D460V constructs (Figure 2, A and B). The D460V mutant is impaired in its MHD motif critical for ADP binding, thereby hampering nucleotide exchange (Moffett et al., 2002). We predict that this structural relaxation may override the effect of NbGRP7 needed to surpass the activation threshold. Alternatively, the autoactive response may rely on other host components, which may be rate-limiting for the process but are not regulated by NbGRP7. This in turn reflects a degree of specificity for the role of NbGRP7 in NB-LRR signaling that is reliant on effector-induced changes. However, the precise nature of these changes warrants further investigation.

Despite several optimization attempts, we were unable to demonstrate an effect of NbGRP7 on PVX-CP-triggered cell death (Figure 2B). This is fascinating considering that the Rx1-CC and Gpa2-CC domains are highly homologous (95.7% similarity at the protein level). As discussed previously, we cannot exclude that GpRBP-1-induced changes can lead to differences between the effect of NbGRP7 on Gpa2 and Rx1 cell deaths. A likely possibility, however, is that the cell death response by Rx1 is too robust. Thus, residual NbGRP7 from overexpression cannot further boost this response. Furthermore, there is accumulating evidence that cell death is dispensable and can be genetically uncoupled from resistance (extensively reviewed in Künstler et al. (2016)). Likewise, extreme resistance by Rx1 to PVX was postulated to be epistatic to cell death (Bendahmane et al., 1999). This is further reinforced by structure–function studies of the Rx1-CC, indicating that different surface regions of the domain can be linked to cell death and extreme resistance (Slootweg et al., 2018). Thus, we cannot exclude that NbGRP7 may function in regulating extreme resistance while having a limited role in the cell death pathway. Similar outcomes were noted for GLK1, whose overexpression only impacts extreme resistance as well (Townsend et al., 2018).

Co-ordinated control of plant NB-LRRs transcripts is key for appropriate defense activation. This has led to an extensive evolution of various molecular checkpoints to fine-tune the dosage of NB-LRRs in the cell. As a corollary, there is ample evidence for splicing, lifetime, and export of mRNAs as a differential response to biotic stress (extensively reviewed in Lai and Eulgem (2018)). AtGRP7 was shown to bind directly to transcripts encoding Pattern-Recognition Receptors *in vivo*, although the consequence of such bindings remains unclear. Here, we demonstrate that overexpressing NbGRP7 enhances the transcript and protein levels of intracellular Rx1 (Figure 4). Earlier studies performed in potato protoplasts have shown that the extreme resistance response of Rx1 to PVX does not require *de novo* synthesis

of defense transcripts (Gilbert et al., 1998). In this model, it is, therefore, imperative that a sufficient pool of preexisting components is available for defense. This puts posttranscriptional regulation at the forefront for regulating Rx1 function. Furthermore, this is in accordance with reports demonstrating that Rx1 transcripts are subject to regulation by 22-nt microRNAs (Li et al., 2012). Previous works in potato have shown that modulating Rx1 and Gpa2 transcript/protein abundance directly impacts defense output (Slootweg et al., 2017), indicating that exerting control at a posttranscriptional level is important in fine-tuning immunity. We believe that the biological role of plant GRP7s as RNA chaperones fit within this framework. Consistent with this, we observed that the interaction of NbGRP7 and Rx1 localize to speckle-like structures in the nucleoplasm (Figure 1B) that are linked to active sites of (post)-transcriptional processing (Spector and Lamond, 2011).

Although the mechanistic basis of how NbGRP7 contributes to Rx1 and Gpa2 at a posttranscriptional level is not fully clear, functional studies with the NbGRP7 R49K/R49Q mutant variants indicate that its RNA binding capacity is involved (Figures 3, 4, D and F). Thus, it will be of interest to determine whether NbGRP7 directly impacts the turnover of Rx1/Gpa2 transcripts as described for AtGRP7 and FLS2 (Nicaise et al., 2013). Imaginably, NbGRP7 could also concurrently regulate multiple targets, for example, defense-transcripts downstream of Rx1. This is reminiscent with the regulation of PR-1 by AtGRP7 does not involve direct binding to the PR-1 transcript (Hackmann et al., 2014). Preliminary data show that NbGRP7 overexpression upregulates a number of defense marker genes (Supplemental Figure S10). Hereby, it is important to note that our expression analysis did not indicate any nonspecific impacts on the housekeeping gene actin, thus the effect is specific in response to immunity. Future studies should, therefore, aim at elucidating the nature of the immediate cargo bound to NbGRP7.

Despite the pro-immune function of NbGRP7, the down-regulation of GRP7 upon PVX or *G. pallida* infection (Figure 5) may due to ETI suppression by PVX or *G. pallida*, a phenomenon often observed for pathogens to overcome PTI and ETI responses (Abramovitch and Martin, 2004; Goverse and Smant, 2014; Asai and Shirasu, 2015). This counter defense response is further supported by the observation that the RNA-binding function of AtGRP7 is targeted by the *P. syringae* effector HopU1 to promote virulence of the bacteria (Fu et al., 2007). Although the *P. syringae* effector HopU1 can target AtGRP7 to affect the RNA binding between AtGRP7 with FLS2 transcripts, HopU1 does not affect the AtGRP7-FLS2 protein–protein interaction (Nicaise et al., 2013). Moreover, AtGRP7 is able to associate with several translational components, such as eIF4E and the ribosomal subunit S14 (Nicaise et al., 2013) suggesting a potential role of AtGRP7 in the translational machinery. For this reason, we could not exclude a possibility that GRP7 regulates Rx1 and Gpa2 functioning at the translational level. This may

occur independent of GRP7 RNA-binding capacity, which may explain the contribution in Rx1 and Gpa2 functioning but an observed downregulation of GRP7 upon PVX or *G. pallida* infection.

Altogether, we envision that NbGRP7 belongs to a complex that regulates the transcript homeostasis of the NB-LRR Rx1 and Gpa2, and associated defense genes for immunity (Figure 6). By docking to the Rx1/Gpa1-CCs, NbGRP7 arrives in close proximity to other bound interactors in the receptor complex. In the case of Rx1, this may refer to cytoplasmic RanGAP2, which coincides with our observation that NbGRP7 does not share an interacting surface with RanGAP2 on the Rx1-CC (Supplemental Figure S4 A and B) (Sacco et al., 2007; Tameling and Baulcombe, 2007). Alternatively, NbGRP7 may be brought in close proximity to other nuclear components like GLK1 and DBCP at the DNA to regulate the function of Rx1 in the nucleus (Fenyk et al., 2015; Townsend et al., 2018; Sukarta et al., 2020). For example, when Rx1 induces transcriptional reprogramming via the activity of transcription factors such as GLK1, NbGRP7 can stabilize the resultant transcripts and thereby, safeguards

response outputs. It would, therefore, be fascinating to determine how NbGRP7 would co-operate with existing nuclear interactors of Rx1 and contribute to the transcriptional regulation of downstream immune responses.

## Materials and methods

### Plasmid construction

Full-length NbGRP7 was isolated from *N. benthamiana* cDNA using gene-specific primers listed in Supplemental Table S2 as a NcoI–KpnI fragment by High Fidelity PCR (Promega, Madison, WI, USA) according to the manufacturer's protocol. Purified fragments were initially ligated into pGEMT-easy for sequencing and then sub-cloned into the pRAP vector (Schouten et al., 1997) containing the N-terminal 4×Myc.GFP tag by 3-way ligation (1:1:1 ratio) following additional BspHI digestion reactions. Positive clones were finally cloned into the pBINPLUS binary vector (van der Vossen et al., 2000) as AscI–PacI fragments in *A. tumefaciens* MOG101. The full-length nucleotide sequence of NbGRP7 was deposited in Genbank with accession MW478352.

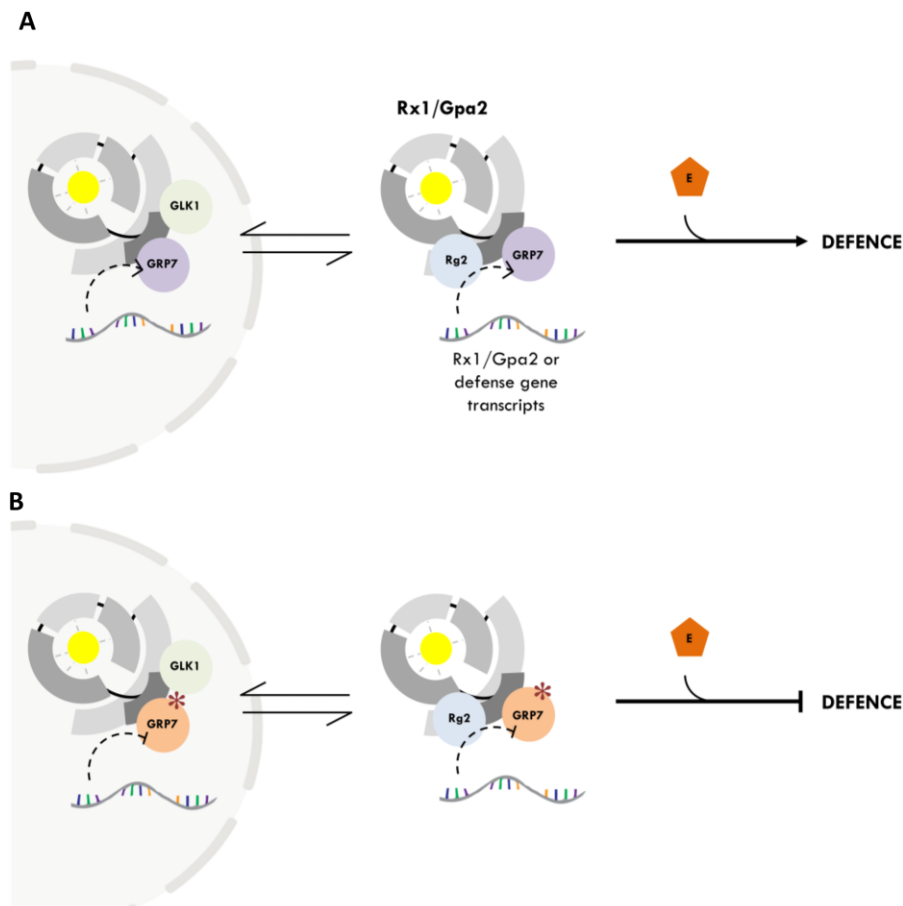


**Figure 6** Schematic representation of a working model proposed for the role of NbGRP7 in ETI by Rx1/Gpa2. A, NbGRP7 exists as preformed complexes with the receptor proteins in either the nucleus and/or cytoplasm. NbGRP7 is presumed to regulate the transcript and protein levels of Rx1/Gpa2 and/or defense components in the cell through its RNA chaperone activity via a yet undefined mechanism (curved dashed line). Presence of the appropriate elicitor (E) is recognized in the cytoplasm and triggers a conformational switch in Rx1/Gpa2. Collectively, these changes ensure that a balanced and steady abundance of Rx1/Gpa2 is present to promote an immune response. B, Impairing the RRM of NbGRP7 (asterisks) is predicted to compromise its ability to regulate the target transcripts, thereby compromising defenses by Rx1/Gpa2.

For targeted substitution of NbGRP7 R49Q and R49K, nested PCR was performed using primers listed in [Supplemental Table S2](#) and Ready-ToGo beads (Illustra PuReTaq PCR Beads, GE Healthcare, Chicago, IL, USA). In the first round, primers were used to amplify regions encompassing the mutation in the RRM. The resultant fragment was used as template in a second round of PCR with overlapping extensions to obtain the full-length NbGRP7 fragment. The same cloning steps for addition of 4×Myc.GFP tag and into the binary pBINPLUS vector was performed as listed above.

For hairpin silencing, potential silencing regions in NbGRP7 were screened using the Solgenomics VIGS tool (<http://solgenomics.net/tools/vigs>) against the *N. benthamiana* gene models database version 04.4. Selection of optimal regions included least probability of off-target effects. Target sequences were ordered synthetically (Genscript Biotech BV, Leiden, the Netherlands) in antisense orientation with a spacer in between as specified in [Supplemental Table S3](#). These were sub-cloned into the destination vector pPT2 (Shin et al., 2017) by BamHI/XbaI digestion first in *Escherichia coli* TOP10 and finally, *A. tumefaciens* strain MOG101.

For BiFC, NbGRP7, Rx1-CC, and Gpa2-CC were cloned initially into pENTR-D topo vector (Invitrogen, Waltham, MA, USA). Sequence-verified fragments were then cloned into both pDEST-SCYNE(R)<sup>GW</sup> or pDEST-SCYCE(R)<sup>GW</sup> vectors by Gateway LR reaction as described (Gehl et al., 2009; Diaz-Granados et al., 2020).

### ATTA

ATTA was used as a system for heterologous protein expression in plants as described in [Slootweg et al. \(2010\)](#). Final agrobacterial suspensions were diluted to final optical density (OD<sub>600</sub>) values according to each assay. Agroinfiltration was performed on the underside of the leaves of 2–3 weeks old *N. benthamiana* plants using needleless syringes. Plants were grown under standard glasshouse conditions at a constant temperature of 23°C with light and dark cycle of L18:D6. Infiltrated spots were screened for the development of cell death, harvested for protein extraction, or examined by microscopy at 1–5 dpi depending on the assay and construct.

### Protein extraction and immunodetection

Protein extraction was performed as described in [Slootweg et al. \(2010\)](#). Briefly, 50–100 mg of leaf material was grounded in extraction buffer (10-mM DTT, 150-mM NaCl, 50-mM Tris-HCl, pH 7.5, 1-mM EDTA, 10% v/v glycerol, 2% w/v polyvinylpyrrolidone, and 0.5-mg/mL pepabloc SC protease inhibitor [Roche, Basel, Switzerland]), and spun down at 16,000 rpm for 5 min at 4°C. The supernatant was run through a G25-sephadex column and the eluate was used for subsequent pull-down assays or mixed directly with 4X Nupage LDS sample buffer with 1M DTT (Invitrogen). Proteins extracted were then separated by loading onto 12% Sodium dodecyl sulfate-polyacrylamide gel electrophoresis

(SDS-PAGE) run in 1X MOPS buffer and visualized by Commassie Brilliant Blue (CBB) staining or wet blotting. Myc-tagged candidate interactors were detected using Goat  $\alpha$ -Myc polyclonal antibodies (Abcam, Cambridge, UK) in subsequent protein blot analysis as described by [Tian et al. \(2014\)](#). However, hereby immunodetection was achieved using a second polyclonal antibody conjugated with Horse-Radish Peroxidase (Abcam, Cambridge, UK). Conversely, HA and GFP-tagged fusion proteins were detected using a Peroxidase-conjugated  $\alpha$ -HA (Roche, Basel, Switzerland) or  $\alpha$ -GFP (Abcam, Cambridge, UK) antibodies respectively. Finally, peroxidase activity was detected by reacting with the Dura luminescent and SuperSignal West Femto substrates (1:1 ratio; Thermo Scientific, Pierce, Waltham, MA, USA) using the G:Box gel documentation system (Syngene, Cambridge, UK).

### In planta Co-IP assays

N-terminally tagged constructs for expression of p35S:Rx1-4×HA.GFP, p35S:Rx1 S1-4×HA.GFP, p35S:Rx1 S4-4×HA.GFP, p35S:4×HA-Rx1 CC S1, p35S:4×HA-Rx1 CC S4, p35S:4×HA-Rx1.CC, p35S:4×HA-Gpa2.CC, p35S:4×HA.Gpa2, and p35S:4×HA.GFP were as described in [Slootweg et al. \(2010\)](#) and [Slootweg et al. \(2018\)](#). *Nicotiana benthamiana* leaves infiltrated by the appropriate protein combinations (at OD<sub>600</sub> of 0.3–0.5) were harvested at 2–3 dpi. For Co-IP, proteins were extracted as described above. Prior to the pull-down, protein samples were precleared by incubation with mouse IgG1 agarose beads. After mixing with  $\alpha$ -GFP,  $\alpha$ -Myc, or  $\alpha$ -HA magnetic beads ( $\mu$ MACS) and washing, eluted proteins were run in an SDS-PAGE system (Bis-Tris gel, 12%, Invitrogen) with 1× 3-(N-morpholino)propanesulfonic acid (MOPS) buffer and blotted onto polyvinylidene fluoride (PVDF) membrane. Immunodetection was then performed as described beforehand using the appropriate antibodies.

### Co-IP/MS analysis

For proteomics analysis, p35S:Gpa2.CC-GFP or p35S:GFP was expressed transiently in *N. benthamiana* between 22 and 28 h. Proteins were extracted from leaf samples as detailed previously and used in cell fractionation as described in [Slootweg et al. \(2010\)](#). Bait proteins were precipitated using  $\mu$ MACS  $\alpha$ -GFP beads (Miltenyi Biotec, Leiden, the Netherlands) as described above. Peptides were generated by on-beads trypsin digestion of the pull-down samples, which were subsequently sent for MS analysis at the Proteomics Centre at WUR Biochemistry (Wageningen, the Netherlands). For identification of proteins, the spectra of each run was matched using MaxQuant software via a database consisting of translated ESTs and UniProt data referring to *N. benthamiana* and tobacco (*Nicotiana tabacum*).

### Confocal laser scanning microscopy

Cellular localization studies were performed using the Zeiss LSM 510 or the Leica SP8-SMD confocal microscope (for BiFC experiments). Agrobacteria harboring the appropriate

constructs were infiltrated on *N. benthamiana* leaves at final OD<sub>600</sub> values of 0.3–0.5. Leaf epidermal cells were harvested at 2–3 dpi for imaging as described previously in [Slootweg et al. \(2010\)](#). In general, Argon laser (intensity ranged from 5% to 8%) was used to excite GFP at 488 nm and GFP was detected (gain ~1,000) at emission wavelength of 470–550 nm. For BiFC measurements, the white laser (CFP laser intensity ranges from 5% to 10%) was used to excite SCFP3A and chlorophyll auto-fluorescence at 440 and 514 nm, respectively. SCFP3A was detected at emission wavelength of 448–495 nm. Chlorophyll auto-fluorescence was detected at emission wavelength of 674–695 nm. Analysis of fluorescence intensities was performed using the ImageJ application software.

### Chlorophyll assay

Chlorophyll content was measured to indicate degree of cell death as described previously in [Harris et al. \(2013\)](#). Briefly, 3 mm discs of infiltrated *N. benthamiana* leaves were incubated overnight in DMSO at 37°C with constant rotation (250 rpm). Subsequently, absorption measurements of the DMSO solution were read at wavelengths 450 and 655 nm using the BioRad Microplate Reader (model 680). Uninfiltrated leaf discs were used as negative controls.

### PVX resistance assay

Viral accumulation was quantified using DAS-ELISA as described in [Slootweg et al. \(2010\)](#). Briefly, plates were coated with polyclonal antibodies (1:1,000) raised against the viral CP (Prime Diagnostics, Wageningen, the Netherlands). A second polyclonal antibody conjugated with alkaline phosphatase was used for immunodetection (1:1,000) at wavelength 405 nm (BioRad Microplate Reader model 680) via the substrate *p*-nitrophenyl-phosphate. Absorbance Measurements were taken with a reference filter of 655 nm.

### Nematode infection assay

Stem segments of the Gpa2 resistant potato genotype SH (*S. tuberosum* ssp *andigena*) were cut and grown in vitro in B5 medium at 22°C under light and dark cycle of L18:D6. Two-weeks later, plant roots were infected with surface-sterilized parasitic juveniles from the potato cyst nematode *G. pallida* (avirulent population D383 or virulent population Rookmaker). Nematode surface sterilization was performed as described ([Goverse et al., 2000](#)). Around 250 infective juveniles were inoculated per root system on single plates in 0.7% (w/v) Gelrite solution. Infected root segments enriched with nematode infection sites were harvested from 15 plants at 3 and 6 dpi and pooled for RNA isolation per time point. Mock inoculation with 0.7% (w/v) Gelrite solution was performed as negative control and samples were collected at 3 and 6 dpi for comparison.

### Expression analysis by RT-qPCR

Total RNA was extracted from 50 mg leaf tissues using the Promega Maxwell 16 simpleRNA extraction kit according to the manufacturer's protocol. First-strand cDNA synthesis

was directly performed using the SuperScript III First-Strand Synthesis System (Invitrogen™). To analyze expression levels, RT-qPCR was done (BioRad System) in a total reaction mix of 25 µL consisting of: 1 µL forward and reverse primers (5 mM each), 8.5-µL Taq ready mix and 12.5 µL MQ water. RT-qPCR was run using the following program: initial denaturation at 95°C for 15 min followed by 40 cycles of amplification at 95°C for 30 s, 60°C for 30 s, 72°C for 30 s and final elongation at 72°C for 60 s with a 90× melting curve at 50°C for 10 s. To promote reproducibility, each sample was analyzed in duplo. In addition, a standard no template control was included to indicate the presence of contaminating DNA. RT-qPCR data were normalized against the actin housekeeping gene. Finally, relative expression levels were analyzed by the comparative method ( $2^{-\Delta\Delta C_t}$ ) using the average threshold values as described in [Schmittgen and Livak \(2008\)](#).

For root material, total RNA was extracted from infected and noninfected root segments using the same RNA extraction kit as used for leaf materials. For reverse transcriptase, cDNA was synthesized with 400 ng of total RNA using the GoScript transcriptase and Oligo-(dT)<sub>12–18</sub> (Invitrogen™). To analyze expression levels, RT-qPCR was done (BioRad System) in a total reaction mix of 10 µL consisting of: 0.5 µL forward and reverse primers (0.5 µM each), 5 µL IQ supermix and 1 µL MQ water. RT-qPCR was run using the following program: initial denaturation at 95°C for 3 min followed by 40 cycles of amplification at 95°C for 30 s, 59.4°C for 30 s, 72°C for 15 s. After amplification, melt curve analysis was run from 65°C to 95°C with a 0.5°C increment every 5 s. Each sample was analyzed in triplo. A standard no template control was included to indicate the presence of contaminating DNA. Two housekeeping genes RPN7 ([Miranda Vde et al., 2013](#)) and TUA5 ([Castro-Quezada et al., 2013](#)) were used for RT-qPCR data normalization. Finally, relative expression levels were analyzed by the comparative method ( $2^{-\Delta\Delta C_t}$ ) using the average threshold values.

### Statistical test

Statistical analyses were performed in R studio version 1.1.456. Data from assays performed in this study were checked for normality using the Shapiro–Wilk test. Depending upon the outcome of the normality test, statistical level was determined either by *t* test or Wilcoxon-signed rank test with  $\alpha = 0.05$ .

### Accession numbers

Sequence data from this article can be found in the GenBank/EMBL data libraries under accession number MW478352 (NbGRP7).

### Supplemental data

The following materials are available in the online version of this article.

**Supplemental Figure S1.** Peptide hits and their locations in the full-length primary sequence of the *NbGRP7* homolog identified in the Co-IP/MS screening.

**Supplemental Figure S2.** Unrooted Bayesian tree of selected orthologs of *NbGRP7*.

**Supplemental Figure S3.** BiFC based interaction analysis of *NbGRP7* and the CC domain of immune receptors Rx1 and Gpa2.

**Supplemental Figure S4.** Pull-down investigating the potential interaction of *NbGRP7* as bait with Rx1 (CC) surface mutants (S1 or S4).

**Supplemental Figure S5.** *NbGRP7* potentiates immunity against PVX avirulent strain (PVX-UK3) independent of Rx1.

**Supplemental Figure S6.** Phenotype of TRV-induced gene silencing (VIGS) of *NbGRP7* in *N. benthamiana* plants.

**Supplemental Figure S7.** Silencing efficiency of *NbGRP7* hairpin silencing constructs.

**Supplemental Figure S8.** Expression of 4×Myc.GFP-*NbGRP7* mutants in planta.

**Supplemental Figure S9.** Identification of *NbGRP7* potato homolog.

**Supplemental Figure S10.** Ectopic expression of *NbGRP7* affects transcript levels of defense marker genes.

**Supplemental Table S1.** Gpa2 Co-IP/MS results.

**Supplemental Table S2.** Primers used in this study as listed according to the assays performed.

**Supplemental Table S3.** Sequences of hairpin constructs used in this study.

## Acknowledgments

We thank Jan-Willem Borst and Arjen Badder from Wageningen Light and Microspectroscopy Centre for providing imaging facilities and their technical expertise, and Martin Cann and Alexander Llewlyn for their biochemical expertise. We are also grateful to Mark Sterken for his advice on the statistical analysis.

## Funding

This work benefits from funding by the Dutch Top Technology Institute Green Genetics (5CFD051RP), Dutch Technology Hotel grant, and the Dutch Technology Foundation STW and Earth and Life Sciences ALW (STW-GG 14529), which are part of the Netherlands Organization for Scientific Research (NWO).

*Conflict of interest statement.* None declared.

## References

- Abramovitch RB, Martin GB** (2004) Strategies used by bacterial pathogens to suppress plant defenses. *Curr Opin Plant Biol* **7**: 356–364
- Asai S, Shirasu K** (2015) Plant cells under siege: plant immune system versus pathogen effectors. *Curr Opin Plant Biol* **28**: 1–8
- Balint-Kurti P** (2019) The plant hypersensitive response: concepts, control and consequences. *Mol Plant Pathol* **20**: 1163–1178

- Bendahmane A, Kanyuka K, Baulcombe DC** (1999) The Rx gene from potato controls separate virus resistance and cell death responses. *Plant Cell* **11**: 781–791
- Bendahmane A, Köhm BA, Dedi C, Baulcombe DC** (1995) The coat protein of potato virus X is a strain-specific elicitor of Rx1-mediated virus resistance in potato. *Plant J* **8**: 933–941
- Bentham AR, Zdrzalek R, De la Concepcion JC, Banfield MJ** (2018) Uncoiling CNLs: Structure/Function Approaches to Understanding CC Domain Function in Plant NLRs. *Plant Cell Physiol* **59**: 2398–2408
- Bezerra-Neto JP, Araújo FC, Ferreira-Neto JRC, Silva RLO, Borges ANC, Matos MKS, Silva JB, Silva MD, Kido EA, Benko-Iseppon AM** (2020) Chapter 4 - NBS-LRR genes—Plant health sentinels: structure, roles, evolution and biotechnological applications. In P Poltronieri, Y Hong, eds, *Applied Plant Biotechnology for Improving Resistance to Biotic Stress*. Academic Press, Cambridge, MA, pp 63–120
- Bhattacharjee S, Zamora A, Azhar MT, Sacco MA, Lambert LH, Moffett P** (2009) Virus resistance induced by NB-LRR proteins involves Argonaute4-dependent translational control. *Plant J* **58**: 940–951
- Bieri S, Mauch S, Shen QH, Peart J, Devoto A, Casais C, Ceron F, Schulze S, Steinbiß HH, Shirasu K, et al.** (2004) RAR1 positively controls steady state levels of barley MLA resistance proteins and enables sufficient MLA6 accumulation for effective resistance. *Plant Cell* **16**: 3480–3495
- Castro-Quezada P, Aarouf J, Claverie M, Favery B, Mugniéry D, Lefebvre V, Caromel B** (2013) Identification of reference genes for normalizing RNA expression in potato roots infected with cyst nematodes. *Plant Mol Biol Rep* **31**: 936–945
- Chang C, Yu D, Jiao J, Jing S, Schulze-Lefert P, Shen Q-H** (2013) Barley MLA immune receptors directly interfere with antagonistically acting transcription factors to initiate disease resistance signaling. *Plant Cell* **25**: 1158–1173
- de la Fuente van Bentem S, Vossen JH, de Vries KJ, van Wees S, Tameling WI, Dekker HL, de Koster CG, Haring MA, Takken FL, Cornelissen BJ** (2005) Heat shock protein 90 and its co-chaperone protein phosphatase 5 interact with distinct regions of the tomato I-2 disease resistance protein. *Plant J* **43**: 284–298
- Diaz-Granados A, Sterken MG, Overmars H, Ariaans R, Holterman M, Pokhare SS, Yuan Y, Pomp R, Finkers-Tomczak A, Roosien J, et al.** (2020) The effector GpRbp-1 of *Globodera pallida* targets a nuclear HECT E3 ubiquitin ligase to modulate gene expression in the host. *Mol Plant Pathol* **21**: 66–82
- Fenyk S, Townsend PD, Dixon CH, Spies GB, de San Eustaquio Campillo A, Sloopweg EJ, Westerhof LB, Gawehns FK, Knight MR, Sharples GJ, et al.** (2015) The potato Nucleotide-binding Leucine-rich Repeat (NLR) immune receptor Rx1 is pathogen-dependent DNA-deforming protein. *J Biol Chem* **290**: 24945–24960
- Fu ZQ, Guo M, Jeong B-r, Tian F, Elthon TE, Cerny RL, Staiger D, Alfano JR** (2007) A type III effector ADP-ribosylates RNA-binding proteins and quells plant immunity. *Nature* **447**: 284–288
- Gehl C, Waadt R, Kudla J, Mendel RR, Hänsch R** (2009) New GATEWAY vectors for high throughput analyses of protein-protein interactions by bimolecular fluorescence complementation. *Mol Plant* **2**: 1051–1058
- Gilbert J, Spillane C, Kavanagh TA, Baulcombe DC** (1998) Elicitation of Rx-mediated resistance to PVX in potato does not require new RNA synthesis and may involve a latent hypersensitive response. *Mol Plant-Microbe Interact* **11**: 833–835
- Goverse A, de Engler JA, Verhees J, van der Krol S, Helder JH, Gheysen G** (2000) Cell cycle activation by plant parasitic nematodes. *Plant Mol Biol* **43**: 747–761
- Goverse A, Smant G** (2014) The Activation and Suppression of Plant Innate Immunity by Parasitic Nematodes. *Ann Rev Phytopathol* **52**: 243–265

- Hackmann C, Korneli C, Kutyniok M, Köster T, WiedenlÜbbert M, Müller C, Staiger D (2014) Salicylic acid-dependent and -independent impact of an RNA-binding protein on plant immunity. *Plant Cell Environ* **37**: 696–706
- Harris CJ, Sloopweg EJ, Govere A, Baulcombe DC (2013) Stepwise artificial evolution of a plant disease resistance gene. *Proc Natl Acad Sci* **110**: 21189–21194
- Jones JD, Dangl JL (2006) The plant immune system. *Nature* **444**: 323–329
- Jones JDG, Vance RE, Dangl JL (2016) Intracellular innate immune surveillance devices in plants and animals. *Science* **354**: aaf6395
- Kim JS, Jung HJ, Lee HJ, Kim KA, Goh CH, Woo Y, Oh SH, Han YS, Kang H (2008) Glycine-rich RNA-binding protein 7 affects abiotic stress responses by regulating stomata opening and closing in *Arabidopsis thaliana*. *Plant J* **55**: 455–466
- Künstler A, Bacsó R, Gullner G, Hafez YM, Király L (2016) Staying alive – is cell death dispensable for plant disease resistance during the hypersensitive response? *Physiol Mol Plant Pathol* **93**: 75–84
- Lai Y, Eulgem T (2018) Transcript-level expression control of plant NLR genes. *Mol Plant Pathol* **19**: 1267–1281
- Lee HJ, Kim JS, Yoo SJ, Kang EY, Han SH, Yang KY, Kim YC, McSpadden Gardener B, Kang H (2012) Different roles of glycine-rich RNA-binding protein7 in plant defense against *Pectobacterium carotovorum*, *Botrytis cinerea*, and tobacco mosaic viruses. *Plant Physiol Biochem* **60**: 46–52
- Leister RT, Dahlbeck D, Day B, Li Y, Chesnokova O, Staskawicz BJ (2005) Molecular genetic evidence for the role of SGT1 in the intramolecular complementation of Bs2 protein activity in *Nicotiana benthamiana*. *Plant cell* **17**: 1268–1278
- Li F, Pignatta D, Bendix C, Brunkard JO, Cohn MM, Tung J, Sun H, Kumar P, Baker B (2012) MicroRNA regulation of plant innate immune receptors. *Proc Natl Acad Sci USA* **109**: 1790–1795
- Miranda Vde J, Coelho RR, Viana AA, de Oliveira Neto OB, Carneiro RM, Rocha TL, de Sa MF, Fragoso RR (2013) Validation of reference genes aiming accurate normalization of qPCR data in soybean upon nematode parasitism and insect attack. *BMC Res Notes* **6**: 196
- Moffett P, Farnham G, Peart J, Baulcombe DC (2002) Interaction between domains of a plant NBS–LRR protein in disease resistance-related cell death. *EMBO J* **21**: 4511–4519
- Nicaise V, Joe A, Jeong B-r, Korneli C, Boutrot F, Westedt I, Staiger D, Alfano JR, Zipfel C (2013) *Pseudomonas* HopU1 modulates plant immune receptor levels by blocking the interaction of their mRNAs with GRP7. *EMBO J* **32**: 701–712
- Sacco MA, Koropacka K, Grenier E, Jaubert MJ, Blanchard A, Govere A, Smart G, Moffett P (2009) The cyst nematode SPRYSEC protein RBP-1 elicits Gpa2- and RanGAP2-dependent plant cell death. *PLoS Pathog* **5**: e1000564
- Sacco MA, Mansoor S, Moffett P (2007) A RanGAP protein physically interacts with the NB-LRR protein Rx, and is required for Rx-mediated viral resistance. *Plant J* **52**: 82–93
- Schmittgen TD, Livak KJ (2008) Analyzing real-time PCR data by the comparative C(T) method. *Nat Protoc* **3**: 1101–1108
- Schouten A, Roosien J, de Boer JM, Wilmink A, Rosso M-N, Bosch D, Stiekema WJ, Gommers FJ, Bakker J, Schots A (1997) Improving scFv antibody expression levels in the plant cytosol 1The sequences reported in this work have been deposited in the GenBank database. *FEBS Lett* **415**: 235–241
- Shin YJ, Castilho A, Dicker M, Sádío F, Vavra U, Grünwald-Gruber C, Kwon TH, Altmann F, Steinkellner H, Strasser R (2017) Reduced paucimannosidic N-glycan formation by suppression of a specific  $\beta$ -hexosaminidase from *Nicotiana benthamiana*. *Plant Biotechnol J* **15**: 197–206
- Sloopweg E, Roosien J, Spiridon LN, Petrescu AJ, Tameling W, Joosten M, Pomp R, van Schaik C, Dees R, Borst JW, et al. (2010) Nucleocytoplasmic distribution is required for activation of resistance by the potato NB-LRR receptor Rx1 and is balanced by its functional domains. *Plant Cell* **22**: 4195–4215
- Sloopweg EJ, Koropacka K, Roosien J, Dees R, Overmars H, Klein Lankhorst R, van Schaik C, Pomp R, Bouwman L, Helder J, et al. (2017) Sequence exchange between R genes converts virus resistance into nematode resistance, and vice versa. *Plant Physiol* **175**: 498–510
- Sloopweg EJ, Spiridon LN, Martin EC, Tameling WIL, Townsend PD, Pomp R, Roosien J, Drawaska O, Sukarta OCA, Schots A, et al. (2018) Distinct roles of non-overlapping surface regions of the coiled-coil domain in the potato immune receptor Rx1. *Plant Physiol* **178**: 1310–1331
- Spector DL, Lamond AI (2011) Nuclear speckles. *Cold Spring Harb Perspect Biol* **3**: a000646
- Sukarta OCA, Sloopweg EJ, Govere A (2016) Structure-informed insights for NLR functioning in plant immunity. *Semin Cell Dev Biol* **56**: 134–149
- Sukarta OCA, Townsend PD, Llewelyn A, Dixon CH, Sloopweg EJ, Pålsson L-O, Takken FLW, Govere A, Cann MJ (2020) A DNA-binding bromodomain-containing protein interacts with and reduces Rx1-mediated immune response to potato virus X. *Plant Commun* **1**: 100086
- Sun Y, Zhu YX, Balint-Kurti PJ, Wang GF (2020) Fine-tuning immunity: players and regulators for plant NLRs. *Trends Plant Sci* **25**: 695–713
- Takken FLW, Albrecht M, Tameling WIL (2006) Resistance proteins: molecular switches of plant defence. *Curr Opin Plant Biol* **9**: 383–390
- Tameling WIL, Baulcombe DC (2007) Physical association of the NB-LRR resistance protein Rx with a ran GTPase-activating protein is required for extreme resistance to potato virus X. *Plant Cell* **19**: 1682–1694
- Tameling WIL, Nooijen C, Ludwig N, Boter M, Sloopweg E, Govere A, Shirasu K, Joosten M (2010) RanGAP2 Mediates nucleocytoplasmic partitioning of the NB-LRR immune receptor Rx in the solanaceae. Thereby dictating Rx function. *Plant Cell* **22**: 4176–4194
- Tian J, Pei H, Zhang S, Chen J, Chen W, Yang R, Meng Y, You J, Gao J, Ma N (2014) TRV-GFP: a modified Tobacco rattle virus vector for efficient and visualizable analysis of gene function. *J Exp Bot* **65**: 311–322
- Townsend PD, Dixon CH, Sloopweg EJ, Sukarta OCA, Yang AWH, Hughes TR, Sharples GJ, Pålsson LO, Takken FLW, Govere A, et al. (2018) The intracellular immune receptor Rx1 regulates the DNA-binding activity of a Golden2-like transcription factor. *J Biol Chem* **293**: 3218–3233
- van der Biezen EA, Jones JD (1998a) The NB-ARC domain: a novel signalling motif shared by plant resistance gene products and regulators of cell death in animals. *Curr Biol* **8**: R226–R228
- van der Biezen EA, Jones JD (1998b) Plant disease-resistance proteins and the gene-for-gene concept. *Trends Biochem Sci* **23**: 454–456
- van der Vossen EAG, van der Voort J, Kanyuka K, Bendahmane A, Sandbrink H, Baulcombe DC, Bakker J, Stiekema WJ, Klein-Lankhorst RM (2000) Homologues of a single resistance-gene cluster in potato confer resistance to distinct pathogens: a virus and a nematode. *Plant J* **23**: 567–576
- van Wersch S, Tian L, Hoy R, Li X (2020) Plant NLRs: the whistle-blowers of plant immunity. *Plant Commun* **1**: 100016
- Wang L, Yang T, Wang B, Lin Q, Zhu S, Li C, Ma Y, Tang J, Xing J, Li X, Liao H, Staiger D, Hu Z, Yu F (2020) RALF1-FERONIA complex affects splicing dynamics to modulate stress responses and growth in plants. *Sci Adv* **6**: eaaz1622
- Zipfel C (2014) Plant pattern-recognition receptors. *Trend Immunol* **35**: 345–351